ADVANCED MATERIALS TECHNOLOGIES
www.advmattechnol.de

3D-Printed Lipid Mesophases for the Treatment of Chronic Liver Disease

Marianna Carone, Rafaela Gazzi, Remo Eugster, Rita Gelli, Niklaas Manten, Aymar A. Ganguin, Silvia Di Valerio, Garima Yadav, Pasqualina Castaldo, Raffaele Mezzenga, Paola Luciani, and Simone Aleandri**

Although lipid-based formulations are an attractive approach for enhancing the oral bioavailability of lipophilic drugs, their addition into solid oral dosage forms has been proven challenging due to their high viscosity and heat sensitivity. Therefore, unlike the traditional tableting process, this study employed semi-solid extrusion 3D-printing to produce–at room temperature–gastro-resistant printlets containing a high percentage of bioactive lipids for the effective delivery of lipophilic drugs through self-emulsification. The bio-compatible lipidic mesophase ink, owing to a tunable 3D nanostructure, is employed as a starting material to produce printlets via additive manufacturing. An active lipid mixture – with antifibrotic properties – is blended with the antioxidant vitamin E and water, and the ink printability is optimized by carefully tailoring its composition, and thus its phase identity. The obtained printlets disintegrated upon contact with intestinal fluids forming colloidal structures that enhanced the solubility of a poorly water-soluble drug. The printlets exhibited antifibrotic activity on human hepatic stellate cells, LX-2, suggesting that the generated self-emulsified colloidal structures made both the fibrosis-resolving bioactive excipients and the drug promptly available, enhancing their cell uptake and, in turn, their therapeutic activity.

1. Introduction

Lipid-based formulations offer an attractive approach for enhancing the oral bioavailability of several lipophilic drugs[1] thanks to the formation of colloidal particles within the gastrointestinal (GI) tract that ameliorate drug solubility.[2] Despite the commercial and clinical success of various delivery systems,[3] the addition of lipids in solid oral dosage forms has been proven challenging due to their limited versatility with respect to other traditional excipients used to produce tablets.[4] The application of 3D-printing in pharmaceutics and personalized medicine has garnered significant interest in the field.[5–8] Namely, 3D-printing technology enables customizable dosing,[9] manufacturing of polypills,[10–14] and offers tunable drug release.[15–19] This is exemplified by the approval of the first commercially available 3D-printed medication, Spritam, by the United States

M. Carone, R. Gazzi, R. Eugster, N. Manten, A. A. Ganguin, G. Yadav, P. Luciani, S. Aleandri
Department of Chemistry, Biochemistry and Pharmaceutical Sciences
University of Bern
Bern 3012, Switzerland
E-mail: paola.luciani@unibe.ch; simone.aleandri@unibe.ch

R. Gelli
Department of Chemistry "Ugo Schiff" and CSGI
University of Florence
Sesto Fiorentino, Florence 50019, Italy

S. D. Valerio
Department of Clinical and Molecular Sciences
DISCLIMO
University "'Politecnica delle Marche"'
Ancona 60126, Italy

P. Castaldo
Department of Biomedical Sciences and Public Health
University "'Politecnica delle Marche"'
Ancona 60126, Italy

R. Mezzenga
Laboratory of Food & Soft Materials
Institute of Food
Nutrition and Health
Department for Health Sciences and Technology
ETH, Zurich 8092, Switzerland

The ORCID identification number(s) for the author(s) of this article can be found under https://doi.org/10.1002/admt.202301930

DOI: 10.1002/admt.202301930

Food and Drug Administration (FDA) in 2015,[20] which also demonstrated the feasibility of using 3D-printing in large-scale manufacturing.[5,21] Given the high viscosity and heat-sensitivity of lipids, and to facilitate broader drug applicability, our study employs semi-solid extrusion (SSE) 3D-printing technology to produce oral dosage forms containing a high percentage of bioactive lipids for the effective delivery of water-insoluble drugs through self-emulsification. Unlike the traditional tableting process, SSE does not rely on compression forces but instead utilizes a viscous matrix to hold layers of formulation together producing the dosage form at room temperature,[22,23] which is of great importance for thermolabile lipids and active principles. Recently, 3D-printed solid lipid formulations have been described, but to our knowledge always as a blend of lipids and polymers to obviate the suboptimal mechanical properties of the lipids employed.[8,4,12] Here, we selected lipid mesophases (LMPs) as a structured biomaterial to be used as ink for additive manufacturing of 3D printed tablets (printlets).

LMPs are a class of materials belonging to the lyotropic-liquid-crystal family, possessing a tuneable three-dimensional nanostructure along with mechanical and rheological properties (e.g., flexural strength and rigidity) of high interest for efficient material engineering for 3D printing. By altering the water content and temperature or incorporating additives, we can tailor the lipid mesophase to exhibit lamellar (L), cubic (Q), and inverse hexagonal (H_{II}), or micellar geometries.[24] Each phase geometry has an impact on drug release rates, viscosity, and self-emulsification mechanisms. By exploring the nanostructure-property correlations, lipid matrices with the desired material and self-emulsification properties were developed. While extensively investigated – either as bulk gel or as colloidal dispersion – to achieve controlled drug release,[25–28] LMP-based formulations have not been reported so far as starting material to manufacture pharmaceutical oral dosage forms via 3D printing technology. Here, to generate our LMP-based ink (LMP ink) we selected a natural phospholipid from soy, S80, rich in polyenylphosphatidylcholines (PPC) at a concentration greater than 75%. Among the possible candidates able to form LMPs such as phosphatidylcholine, monoacylglycerol lipids (monoolein, monolinolein) and phytantriol, S80 also works as an active ingredient able to deactivate profibrogenic hepatic stellate cells, which are the main collagen-producing cells in hepatic fibrogenesis.[29] Nonetheless, pure unsaturated lipids are unsuitable for 3D-printing due to their intrinsic waxy and soft nature. Therefore, we chose to blend S80 with vitamin E (VitE) because of its demonstrated capacity to promote the formation of a highly viscous gel[30–32] exhibiting an elastic behaviour with a response to shear[33,34] as well as its well-known antioxidant properties that prevent lipid peroxidation.[35]

The poorly water-soluble (logP = 5.7) and highly permeable obeticholic acid (OA; classified as Class II according to the Biopharmaceutics Classification System) represents an ideal active principle to determine the utility of the developed formulation. OA is a semi-synthetic bile acid analogue, acting as agonist of the farnesoid X receptor,[36] and marketed as film-coated tablets approved as orphan medicine for the treatment of primary biliary cholangitis, an autoimmune condition in which there is a gradual destruction of the small bile ducts in the liver.[37] In preclinical studies, OA has also been shown to improve hepatic steatosis, fibrosis, and portal hypertension.[38–41] Despite the encouraging results from clinical studies of their OA tablet formulation Ocaliva against placebo, the company Intercept Pharmaceuticals has been recently denied accelerated approval for the treatment of patients with pre-cirrhotic liver fibrosis due to nonalcoholic steatohepatitis (NASH). Based on the outcome of the randomized global Phase 3 study REGENERATE, US Food and Drug Administration experts concluded that the benefits of Ocaliva do not outweigh the risks in NASH patients with stage 2 or 3 fibrosis. Our recent research on hepatic stellate cells (HSCs), key players in the fibrogenic process, suggests that formulating OA with PPC-based dosage forms could mitigate the possibly detrimental effect of the drug on HSCs and favor a healthy cell phenotype, thus re-igniting the potential of clinical success.[42]

Our approach has led to i) the design of an LMP ink for additive manufacturing containing a high content of bioactive lipid; ii) the incorporation of the water-insoluble OA into the printable LMP ink (OA-LMP ink) at a dose comparable to the marketed one; iii) the production of uniform 3D-printed tablets (printlets) using SSE at room temperature; iv) the disintegration of the printlets in intestinal fluids through self-emulsification and v) the increase in the solubility of the embedded drug in the selected intestinal fluids. Our printlets show potential for the treatment of chronic liver disease and they can serve as a versatile platform for the printing of other poorly water-soluble drugs for oral delivery.

2. Results and Discussion

2.1. LMP Ink Development and Printability Assessment

By exploiting the biocompatible features of LMPs and their material property, we developed a printable ink (LMP ink), which has been further manufactured into printlets with self-emulsifying properties. To achieve successful semi-solid 3D printing using LMPs at room temperature, a careful balance between ink composition, printing parameters, and shape retention is crucial. For a material to be printable, it must exhibit sufficient resistance to deformation to flow through a nozzle and display adequate adhesion to both the build platform and previous layers. At the same time, the material must demonstrate a level of rigidity sufficient to retain its desired shape and support its weight without breaking or collapsing. The phosphlipid S80, which possesses a waxy nature, is unsuitable as printing material.[4] To enhance its printability, water was added as second component but, despite its excellent disintegration behaviour, the binary system S80/water (which shows a lamellar phase -*L*-; **Figure 1a**; Figure S1a, Supporting Information) failed to meet the necessary criteria for printability and shape retention due to the low viscosity of this gel (Figure 1b). A ternary system was then chosen to optimize the ink's mechanical properties. Among the various additives used in LMP engineering, VitE was selected for being a potent lipid-soluble antioxidant[43] able to act as a stiffener of lipid chains[44] and induce phase transition to the more curved inverted micellar and hexagonal phase,[31] associated with rheological properties relevant for the design of printable ink.[32,33] The results show that incorporating a high VitE amount (35%) into the lamellar gel transforms the latter into a highly viscous and non-printable inverse micellar phase (Figure 1a; Figure S1b, Supporting Information). This ink was too viscous and, even at the highest allowed pressure, we were not able to extrude it and print the formulation.

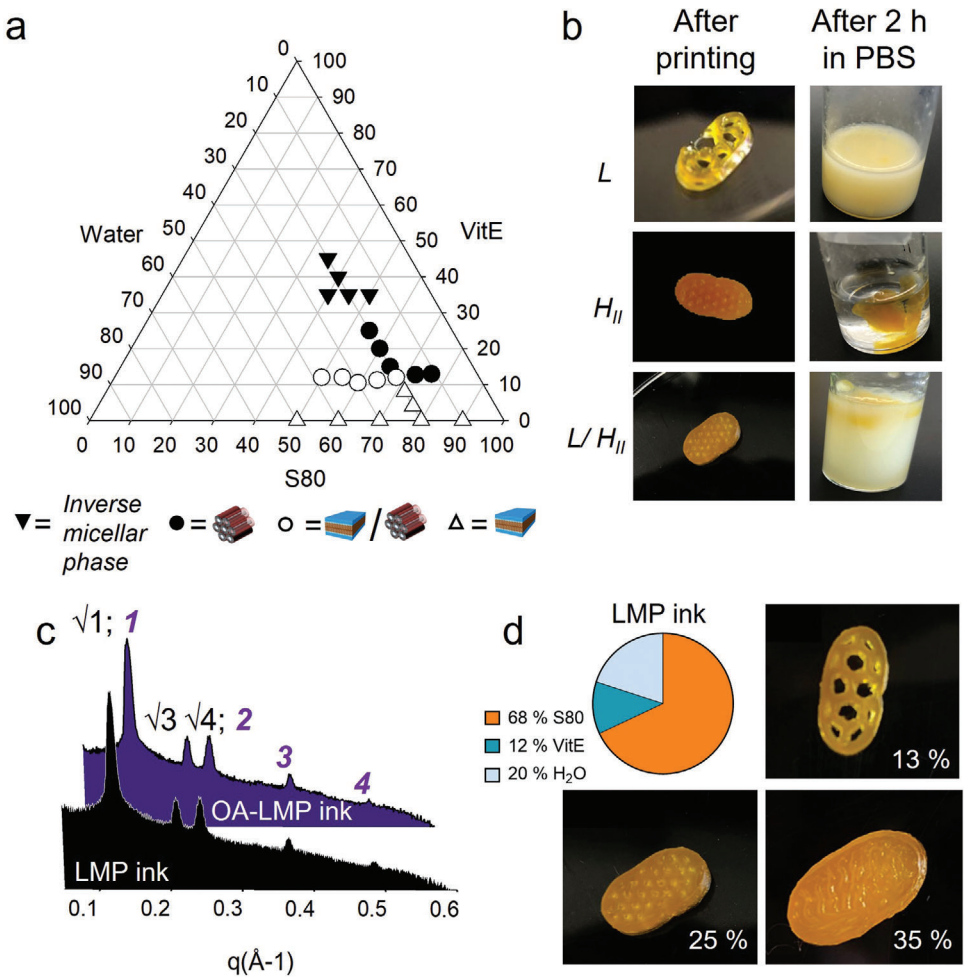

Figure 1. Characterization of the LMP ink and the ensuing printlets. a) Partial phase diagram of the LMP ink composed of S80, water and VitE. The amount of each component in this panel is reported as w/w percentage. The Bragg reflections obtained from the inverse micellar phase do not allow to distinguish between *Fm3m* and *Fd3m* geometry. b) Printlet obtained starting from LMP ink possessing different geometries (*L*, H_{II} and L/H_{II}; top, middle and bottom panel, respectively) and their dissolution behaviour in PBS left colum. c) SAXS spectra of the empty LMP ink and drug-loaded LMP ink OA-LMP ink. The Bragg reflections for the H_{II} $\sqrt{1}$: $\sqrt{3}$: $\sqrt{4}$ and *L* 1: 2: 3: 4 phases are reported above each peak in black and purple, respectively. d) Printlets showing different infill densities obtained from an LMP ink composed of 68% S80, 12% VitE and 20% water, as also reported in the pie chart.

By decreasing the amount of the stiffening agent (at 20%), the gel revealed a pure H_{II} symmetry (Figure 1a; Figure S1c, Supporting Information), whereas keeping on decreasing the VitE amount (12% w/w) the gel showed a coexistence of *L* and H_{II} symmetry (Figure 1a; Figure S1d, Supporting Information). Previous studies confirmed that VitE (with critical packing parameter ≥ 1) can induce this phase transition toward the more negatively curved geometry such as inverted hexagonal and micellar phase.[44] However, the observed coexistence of *L* and H_{II} phases in our LMP ink (at least at the % of S80, VitE and water used) can be explained by a not fully complete phase transition, possibly due to the multiple phospholipid species present in the soy-derived S80. We screened different formulations by varying either the water or VitE content (Table S1 and S2 and Figure S2, Supporting Information). Although both mixed L/H_{II} and pure H_{II} inks were printable, the H_{II}-based ink did not dissolve in PBS after 2 h of incubation, whereas the gel where *L* and H_{II} coexisted completely disintegrated in buffer after 2 h (Figure 1b). Accordingly, a mixed phase composed of the highest S80 amount (68% w/w) and OA at a concentration of 2.5% w/w (based on commercially available tablets[45]) embedded in it (OA-LMPs ink) was further investigated. Notably, its incorporation into the LMP ink did not result in any additional phase transition since the sequence of Bragg reflections for a *L* and H_{II} phase (1:2:3:4 and $\sqrt{1}$:$\sqrt{3}$:$\sqrt{4}$, respectively) coexisted as determined in the case of empty ink (Figure 1c).

The LMP ink was extruded through a 27G nozzle, producing oval tablets utilizing a honeycomb geometry, as depicted in Figure 1d. The end product was a yellow-colored tablet, due to the presence of the S80 lipid mixture, and no solidification or dripping was observed during the printing process. Moreover, the honeycomb geometry was modified by controlling the infill densities (13%, 25%, and 35%), and hence surface area, to enable, for example, dose personalization without the need to alter

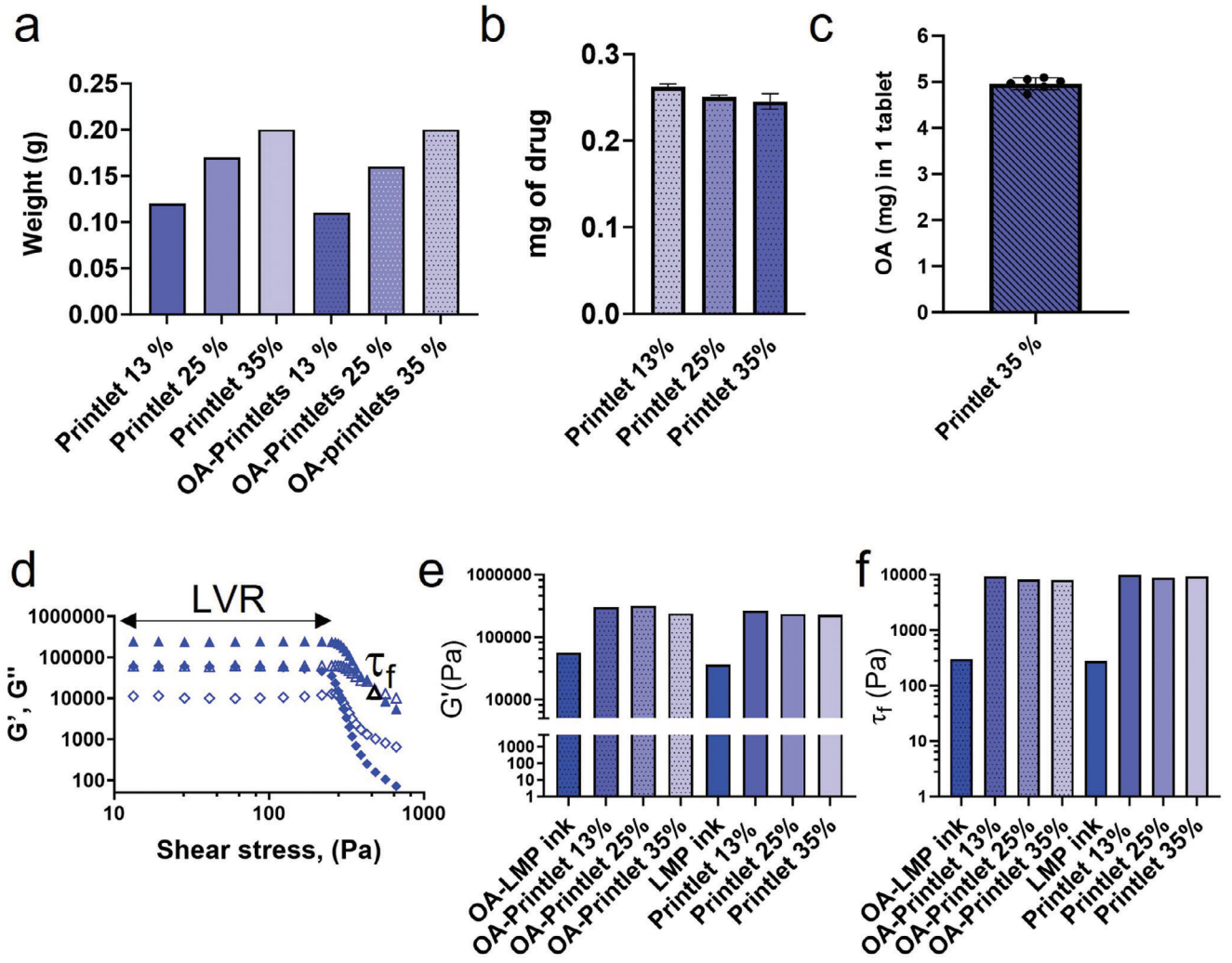

Figure 2. Characterization of empty and OA-loaded LMP ink and printlets. a) Mass of printlets with different infill density with and without OA (solid bars and bars with pattern, respectively). b) Mass of drug expressed in mg) present in a batch of printlets 10 mg) with different infill densities. c) Drug amount present in one printlet with infill density 35%. d) Representative amplitude sweep graph for the LMP ink (diamonds) and printlet at 35% infill density (triangles); G′- filled symbols and G″- empty symbols. The linear viscoelastic region (LVR) and the flow point τ_f are represented as an arrow and a white triangle. e) G′ represented as mean of G′ values in the LVR of LMP ink and printlets with and without OA (solid and bars with patterns, respectively) at different infill densities and f) flow points τ_f of LMP ink and printlets with and without OA (solid and bars with patterns, respectively) at different infill densities. The values in panels b and c are reported as mean ± STDV n ≥ 3).

the formulation. While exploring the industrial scalability of the process was not the target of our study, it is worth noting that the 3D printer employed here does not allow us to print industrial batches, yet the process can be scalable. Indeed, the parameters (pressure and speed) fixed within this work can be used in a further scale-up study aimed at translating the R&D process into an industrial scale. Following 24 h of drying at room temperature, the printlets displayed suitable mechanical properties (e.g., flexural strength and rigidity) for handling without the risk of breaking or deformation. Immediately after printing and after 24 h at room temperature, the printlets were weighed and during this period only a slight change in their weight was observed (Figure S3, Supporting Information). Both SAXS spectra of the ink (Figure 1 panel c) and 24 h after printing (see **Figure 2** panel c) showed a coexistence of H_{II} and L phases. The only appreciable difference is the shift of the first reflection at higher q in the case of dry printlets, which indicates a minimal water loss. Interestingly, SAXS spectra recorded on different batches of printlets are identical, highlighting the good homogeneity of the ink and the robustness of the printlet preparation. Only a negligible amount of residual methanol (1.22 ± 0.22 μg printlet^{-1}) was detected in our printlets, confirming the suitability of the production protocol for further preclinical and clinical use. As for the ink, the presence of OA did not affect the printing parameters, which were identical to those used for the manufacturing of empty printlets (Figure S3, Supporting Information). However, as expected, by increasing the infill density, and thus the amount of LMP ink deposited in the honeycomb geometry, we observed a

2-fold increase in weight for printlets from an infill density 13% to 35% (see **Figure 2**a).

Drug distribution within the OA-Printlets of various infill densities was carried out to assess the homogeneity of the solid dosage forms. As shown in Figure 2b, the drug distribution throughout the tablets with different infill densities was consistent and uniform, highlighting the favourable properties of LMPs in the additive manufacturing of high-dose tablets. The consistent drug loading during the printing process precluded any settling or aggregation of the drug in the printer cartridge. The OA-Printlets with infill density 35% were formulated with 5 mg of OA, a dose comparable to commercially available tablets and the total measured drug content shows a strong correlation with the theoretical value (Figure 2c).

To investigate the impact of either the printing process or the presence of OA on the viscoelastic properties and the structural strength of the LMP ink, we conducted rheological (amplitude sweep) measurements on LMP ink prior to and following the manufacturing of printlets at various infill densities. Either in the LMP ink or in the printlets (with and without OA) the shape of G′ and G″ (the storage and loss of moduli, respectively) exhibit a sharp downturn at the limit of the linear viscoelastic region (LVR), above that a strain increase causes the disruption of the network, resulting in a decrease of both G′ and G″ as evident in the representative graph shown in Figure 2d (and Figure S4, Supporting Information). This phenomenon was previously interpreted with a "slip-plane" model,[46–48] which suggests that large deformations occur along certain planes in the structure while maintaining relatively small deformations elsewhere. Interestingly, following the printing process, the G′ value in the LVR increases indicating a higher structural strength (Figure 2e). The flow point, which also serves as a parameter for assessing the structural strength of the material (and it is related to the required force to be applied on the sample to induce flow), confirms that the LMP ink has a low rigidity, (Figure 2f) property crucial for the optimal flexural strength needed for the material to flow through the nozzle while maintaining shape after printing. Moreover, in the case of printlets, G′ dominated over G″ also varying the frequency range, thus indicating strong stability of the material over time (Figure S5, Supporting Information).

2.2. Printlet Behavior in the GI Tract and Assessment of Self-Emulsification

Lipid-based formulations are generally employed to enhance the solubility of embedded (lipophilic) drugs through the formation of various colloidal structures. In the development of either LMP ink or the resulting printlets, we sought to explore the formulation behaviour and its self-emulsifying properties within the GI tract. As depicted in **Figure 3**a, we also considered the different environments that an oral dosage form, and thus a drug, needs to bypass before reaching its target organ.

It is worth noting that the printlets do not dissolve in the simulated stomach acidic environment (Figure 3b) and the active lipid is not degraded (Figure S6, Supporting Information) while the ink's internal structure transforms into an inverse micellar structure (Figure 3c). Although at low pH the surface area of the lipid might change, thus changing its critical packing parameter and, in turn, the LMP ink symmetry,[49,50] macroscopically this acidic condition does not erode the printlet which shows an increase in weight after incubation for 2 h in HCl due to the swelling of the LMP ink. Following the journey of the oral dosage into the GI tract, the emulsification behavior of printlets upon exposure to fasted-state simulated intestinal fluid and fed-state simulated intestinal fluid (FaSSIF and FeSSIF, respectively) as well as to plain buffer in the form of PBS at pH 7.4 was assessed, too. As shown in Figure 3d, the printlets were fully emulsified within 2 h (at 37 °C) in all three media, with traces of undissolved fragments observed only in the presence of plain buffer.

When the printlets were exposed to FaSSIF and FeSSIF, the resulting media was relatively homogeneous with no clumps and the dynamic light scattering (DLS) analysis revealed a highly polydisperse dispersion with multiple species in solution (Table S3, Supporting Information). Cryo-TEM images were acquired to gain further insight into the emulsification process (Figure 3e). In PBS, the media was dominated by the presence of lipid droplets, vesicles and large colloidal crystalline structures (internally ordered), compatible with a dispersion of the parental bulk gel. The presence of bile components in FaSSIF resulted in a polydisperse media containing micelles, vesicles, multilamellar vesicles, and lipid droplets of varying size and morphology. In agreement with a previous study,[51] FeSSIF showed a higher abundance of vesicles, potentially due to the presence of surfactants such as taurocholic acid and lecithin, along with pancreatin. In general, these results strongly suggest that the use of biorelevant media lowers the degree of structural order of the bulk printlets (and their parent LMP ink), as also established by the absence of Bragg reflections in the SAXS spectra performed on the media (Figure S7, Supporting Information). On the contrary (and as previously envisioned; Figure 1b) the pure H_{II} ink (composed of 65% S80; 15% VitE and 20% water) was found to be completely insoluble in PBS, while the pure L phase (80% S80 and 20% water) reaches immediately complete dissolution (Figure S8, Supporting Information). Therefore, we hypothesized that the lamellar component (present in our LMP ink) may act as a trigger for disintegration, facilitating the rapid dissolution of the tablet upon exposure to the aqueous media and the transition from a crystalline structure to a less ordered vesicle based-dispersion.

2.3. Equilibrium Solubility and Drug Release Assessment

Aiming to determine the equilibrium solubility of OA and the impact of the formulation, we performed experiments to evaluate the solubility of free drug and OA-Printlets in three different dissolution media: PBS, FaSSIF, and FeSSIF. As showed in **Figure 4**a, the complete solubilization of the drug was only achieved when OA was incorporated into the printlets and in the presence biorelevant media. In this condition, lecithin, taurocholate acid, and bile acids interact with the formulation forming a range of colloidal structures that help to reduce precipitation and maintain the drug in a solubilized state, as previously reported.[52–55] In comparison, the solubilization of free OA was always incomplete,[56] and its incorporation into the formulation did not significantly improve the solubility in plain buffer. Moreover, our formulation can provide additional benefits in terms of drug release, potentially controlling the OA absorption.

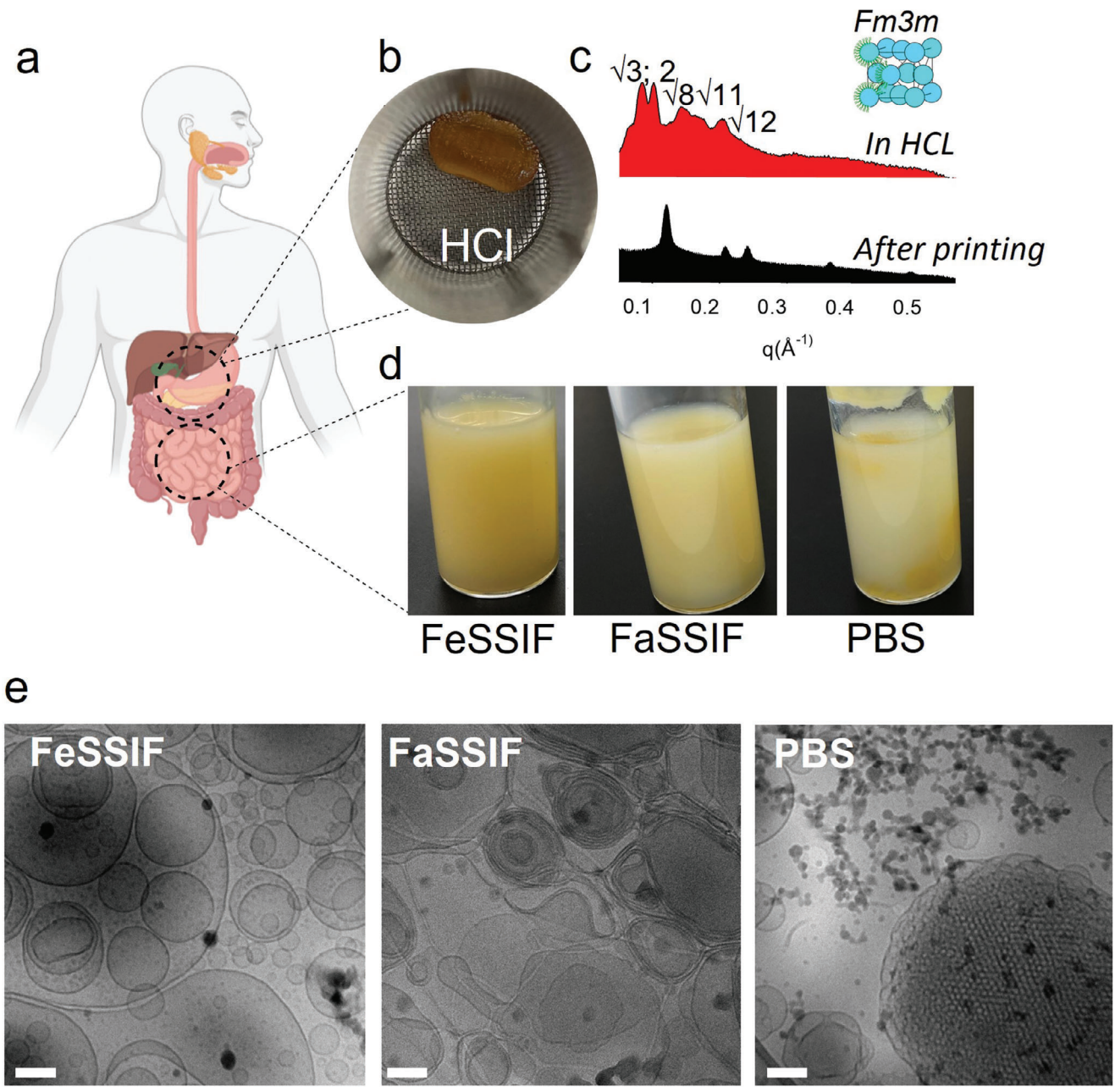

Figure 3. Printlet dissolution into simulated digestive fluids. a) Schematic representation of the different GI tract locations. b) Printlet after 2 h in HCl at 37 °C and c) its SAXS spectra, where the Bragg reflections identify an inverse micellar phase with a *Fm3m* geometry $\sqrt{3}$: 2: $\sqrt{8}$: $\sqrt{11}$: $\sqrt{12}$). d) Printlets after 2 h in intestinal media FeSSIF and FaSSIF) and plain PBS at pH 7.4 and e) their corresponding cryo-TEM images. The scale bar corresponds to 100 nm.

A release experiment was carried out and drug-loaded formulations were placed in the custom-made basket. As evident from the OA release profile (Figure 4b), the 3D gel network retains the OA allowing its slow and controlled release.

To better simulate the disintegration of the printlets and thus the drug release in physiological conditions, we carried out a more dynamic and multi-phase in vitro experiment. Here, the printlets were first kept in HCl for 1 h (at pH 1.2 to mimic the stomach) in a metal mesh basket and then transferred into a biorelevant media (FaSSIF) enriched with pancreatin, as previously reported.[57] The internal structure of the ink first transformed into an inverse micellar structure in the stomach environment while, in the presence of pancreases, the Bragg reflections for a lamellar phase (1: 2: 3; reported above each peak in bold) coexisted with those of inverse micelle (Figure 4 panel c). Increasing the incubation time, the enzyme promoted a destabilization of ink's internal structure as confirmed by the decrease of scattering intensity and by a low resolution of the Brag's

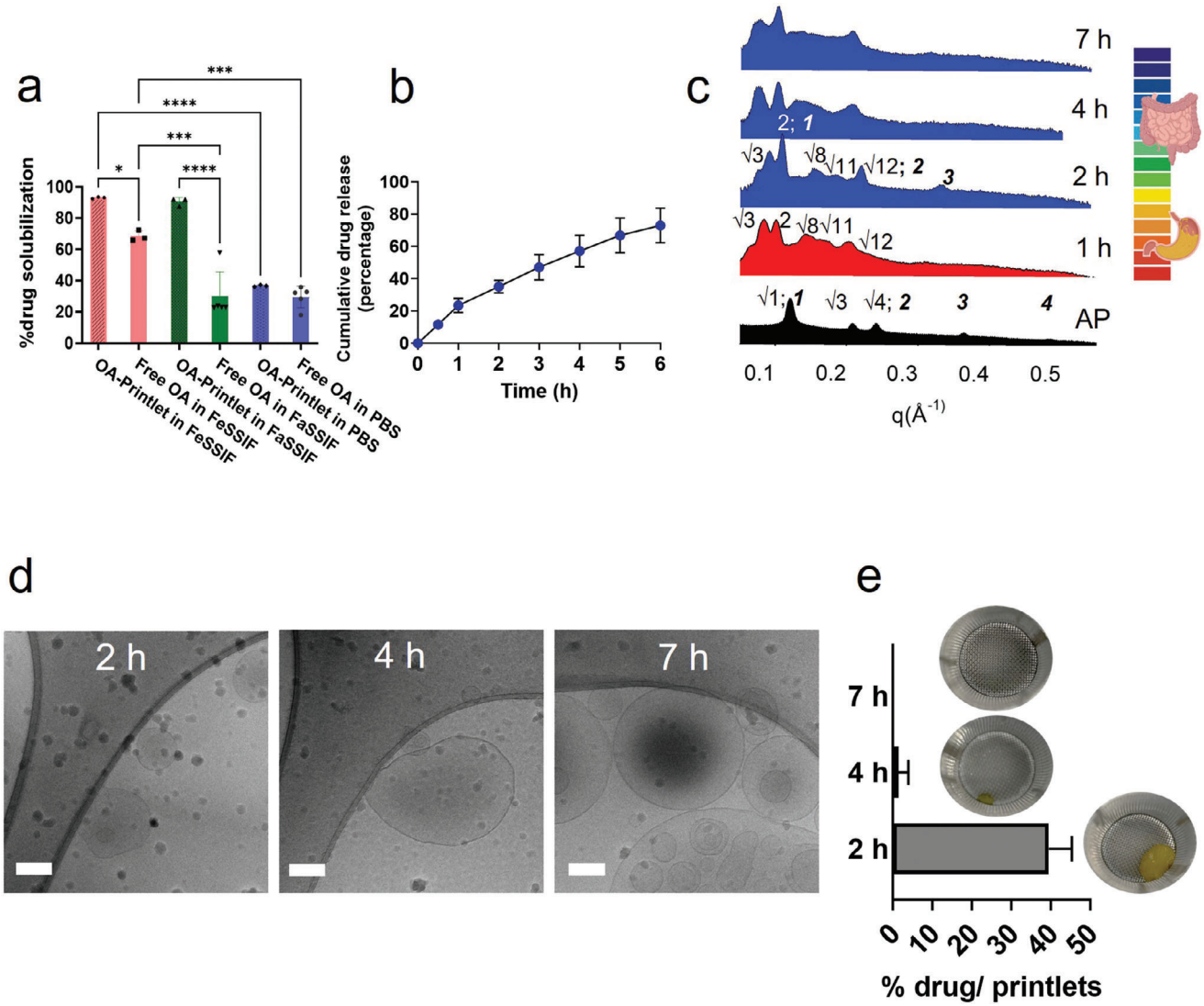

Figure 4. Equilibrium solubility of OA as free drug (Free OA; solid bars) and printlet containing OA (OA-Printlet; bars with pattern) in different dissolution media a) and OA release profile from a printlet with 35% infill density in PBS b). Dynamic and multi-phase in vitro experiment to better simulate the disintegration of the printlets: c) SAXS spectra acquired at different time points: immediately after printing (AP, black spectrum); after 1 h in HCl (red spectrum); and after 1, 3 and 6 h in biorelevant media FaSSIF enriched with pancreatin (blue spectra); d) Cryo-TEM images of the release media at different incubation time (the scale bar corresponds to 100 nm); e) amount of OA present in each printlet expressed as percentage) after 2, 4 and 7 h incubation in biorelevant media FaSSIF enriched with pancreatin. The pictures above the bars in the plot show the residual amount of printlet present at the specific time point. The values in panels a, b, and e are reported as mean ± STDV n ≥ 3). *$p < 0.05$, **$p < 0.01$, ***$p < 0.001$ as determined by one-way ANOVA with multiple comparisons and Tukey correction. All tests were performed using Prism GraphPad) and applying default settings for the above-mentioned analyses.

reflections in the spectra acquired after 7 h. Cryo-TEM images of the release media at different incubation times (Figure 4d) confirmed the dynamic structural changes of the LMPs induced by pancreatin. A variety of similar aggregates (micelles, vesicles, multilamellar vesicles, and lipid droplets of varying size and morphology) were found in solution with or without pancreatin, but, due to the lipolytic effect of the enzyme, their abundance was tremendously reduced. Moreover, while no drug release was detected in acidic environment after 1 h, the presence of pancreatin completely eroded the printlets, leading to 100% drug release after 7 h (see Figure 4, panel e).

2.4. From Intestinal Absorption to Efficacy in the Treatment of Hepatic Fibrosis

Aiming at increasing OA bioavailability after oral administration and thus reducing liver fibrosis, OA needs to be firstly absorbed into the small intestine (as depicted in **Figure** 5a) and the formulation should not have any adverse effects on the integrity of the intestinal epithelial barrier. As obvious, printlets (and in general solid oral dosage form) cannot be used directly in cell culture; therefore, to circumvent this issue, we treated Caco-2 cell monolayers–mimicking the intestinal epithelium–with

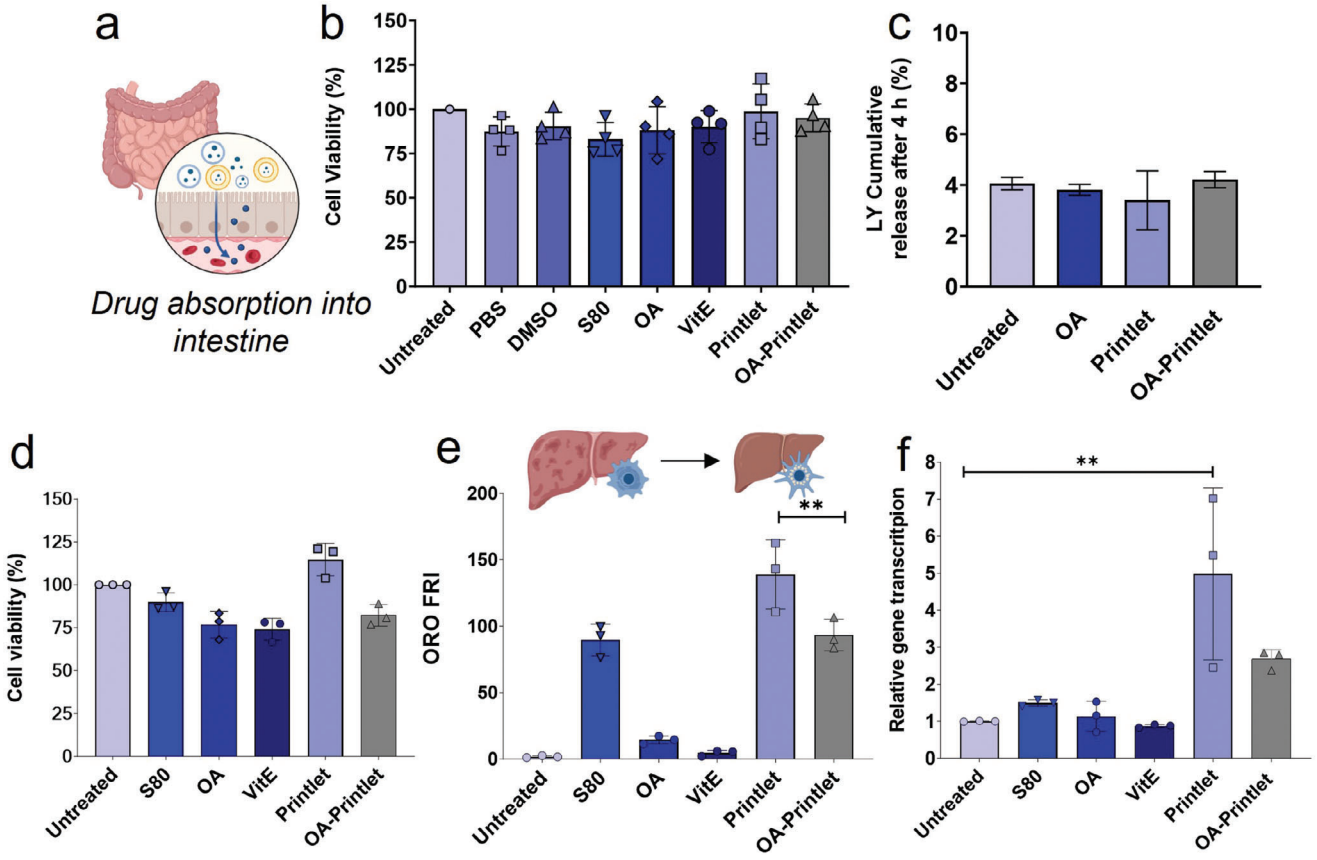

Figure 5. Effect of formulations on intestinal and hepatic cells. a) Differentiated Caco-2 cells mimic the absorption into the small intestine. b) Cell viability of Caco-2 monolayer treated with various formulations. c) Impact of the tested formulations on Caco-2 paracellular transport LY assay. d) Metabolic activity of LX-2 cells in presence of the various treatments. e) Quantification of the Oil Red O fluorescence (ORO FRI) normalized to the number of LX-2 cells in the DAPI field Fluorescent binary area [μm^2]/ cell count. f) Relative mRNA transcription in LX-2 cells of PLIN2 normalized to GAPDH mRNA transcription and normalized to the DMEM condition after different treatments. The values are reported as mean ± STDV n = 3. p-values *** $p < 0.001$, ** $p < 0.01$, * $p < 0.05$ from ordinary one-way ANOVA with post hoc Tukey's multiple comparison analysis. All tests were performed using Prism GraphPad and applying default settings for the above-mentioned analyses.

a media containing the colloidal structure achieved after self-emulsification. Importantly, no discernible cytotoxic effects were observed in comparison to the control (untreated) group. These findings suggest that the tested formulations (and the single components) do not interfere with the viability of the Caco-2 cells (Figure 5b). To further investigate the influence of the formulations on intestinal permeability, we utilized the Lucifer Yellow (LY) assay, a well-established marker for assessing paracellular transport.[58] LY is known to be transported primarily through the paracellular route, making it an appropriate indicator for evaluating tight junction integrity. In our study, we examined the effect of exposure to the emulsion systems and individual components on the permeability of the Caco-2 cell monolayers. Strikingly, no significant changes in paracellular transport or disruption of tight junction integrity were observed upon exposure to the tested formulations after 4 h (Figure 5c). This indicates that the self-emulsifying system and its components did not induce an increase in the permeability of the epithelial cell layers (Figure S9, Supporting Information). Since the results support the potential application of the printlets as a safe and effective approach for enhancing intestinal permeability without compromising cellular viability or barrier, the formulations were further tested in a human HSC cell line, LX-2. Here, we aimed to investigate the antifibrotic response of naïve LX-2 cells when treated with various formulations containing S80, water, VitE, and OA. To establish a comprehensive baseline, we included separate control groups treated with just VitE, OA, S80, and only the cell medium (untreated).

Firstly, the CCK8 assay revealed that the treatment of OA, VitE and the OA-loaded formulation (OA-Printlet) led to a decrease in cell viability by ≈25%, whereas the empty formulation (Printlet) does not affect the cell viability (Figure 5d), a trend in agreement with our previous study.[44] We have already shown that immortalized human LX-2 cells are an ideal system to study the antifibrotic effect of different lipid-based formulations in vitro.[42,59] While activated, fibrotic LX-2 cells are characterized by their loss of lipid droplets following their transdifferentiation into a myofibroblast-like phenotype, their inactivated, quiescent-like counterpart shows an abundance of cytoplasmic lipid droplets, which can be used as a marker. The lipid droplet content was remarkably low after plain OA treatment (Figure 5e), as expected from our previous study,[44] whereas the printlet and

the OA-Printlet exhibited significantly higher signals compared to the background levels. The mRNA transcription analysis of a prominent marker of fibrosis, specifically the expression of PLIN2 gene, coding for the ubiquitously expressed perilipin 2 protein, responsible for neutral lipid storage and metabolism in eukaryotic cells and enhanced in quiescent HSCs[60] confirmed the trends: OA treatment barely increased its expression, on the contrary significantly increased by the printlet (Figure 5f). Overall, the S80-based LMP ink used in this experiment exhibited antifibrotic activity in LX-2 cells and, as observed previously by our group, potentiate the therapeutic effect of an active principle not known to re-establish the quiescent-like phenotype in HSCs. Our results suggest that the prompt availability of fibrosis-resolving bioactive excipients such as PPCs and VitE as self-emulsified colloidal structures once the printlets get in contact with an aqueous medium enhances their cell uptake, their bioavailability, and in turn their therapeutic activity.

3. Conclusion

In our study, we have successfully demonstrated the underexplored potential of lipid mesophases as a printable material suitable for semi-solid extrusion at room temperature. By carefully controlling the ink composition and thus the phase identity of the ensuing ink we can in turn fine tune its rheology and optimize the printability. We were thus able to produce printlets with defined infill densities and overall physical parameters. Our formulation is characterized by a high percentage of a natural phospholipid, generally regarded as safe (GRAS) by the US Food and Drug Administration, with antifibrotic properties, rendering it an exceptional candidate for the delivery of water-insoluble drugs. Upon contact with intestinal fluids, the printlets disintegrated forming colloidal structures that enhanced the solubility of the water-insoluble drug, OA. Remarkably, the printlets and the corresponding 3D structures of the gel are able to retain OA, enabling its slow and controlled release in simulated biorelevant intestinal fluids. Our results suggest that the LMP-based printlets have potential as oral treatment, since the self-emulsifying system generated upon contact with intestinal fluids does not affect either the intestinal cell viability or their permeability. Thanks to the increase in solubility of OA and the co-formulation with known hepatoprotectants such as the PPC-rich S80 and VitE, LMP-based printlets offer a modular playground for the pharmacological treatment of liver fibrosis and can serve as a platform for 3D-printing other poorly water-soluble drugs. The use of LMPs in additive manufacturing paves new avenues not only for multifunctional oral dosage forms but also for bioderived scaffolds based on this material. However, further in vivo studies are needed to test the efficacy of 3D printed formulations using LMP inks. Although the feasibility of using 3D-printing in large-scale manufacturing has been already proven for oral dosage forms such as immediate release tablets, a scale-up study for semi-solid extrusion of purely lipid-based inks is needed to investigate possible bottlenecks in large scale production of LMP printlets.

4. Experimental Section

Materials: S80 with 75% polyenylphosphatidylcholines was a kind gift from Lipoid GmbH (Ludwigshafen, Germany). The specific composition of this lipid mixture was reported in the Supporting Information (Table S5, Supporting Information). VitE (Ph. Eur. Quality) and 3-(4,5-dimethylthiazol-2-yl)−2,5-diphenyltetrazolium bromide (MTT) and porcine pancreatin (8 X USP specifications activity) were purchased from Sigma-Aldrich (St. Louis, USA). OA was purchased from abcr GmbH (Karlsruhe, Germany). Simulated fluids were purchased from Biorelevant (London, UK). Phosphate buffer saline and non-essential amino acids (NEAA) were purchased from Carl Roth (Karlsruhe, Germany). All organic solvents (methanol, acetonitrile, tetrahydrofuran (THF), dimethyl sulfoxide (DMSO) and Lucifer Yellow lithium salt were obtained from Fisher Scientific (Schwerte, Germany). Dulbecco's Modification of Eagle's Medium (DMEM), 1X with 4.5 g L^{-1} glucose, L-glutamine and sodium pyruvate was purchased from Costar Corning (Corning, USA). Penicillin/Streptomycin solution (100X) was purchased from Carlo Erba, L-Glutamine 100X (200 mM) was purchased from Microgem, Fetal Bovine Serum (FBS) and trypsin-EDTA 1X in PBS w/o Phenol Red, w/o Calcium, w/o Magnesium Sterile Filtered were purchased from EuroClone (Milan, Italy). Transwell cellQART 12-well Cell Culture Inserts, 0.4 µm PET clear were purchased from SABEU GmbH (Northeim, Germany). All chemicals were used as received. Ultrapure water of resistivity 18.2 MΩ.cm was produced by a Barnstead Smart2 pure device from Thermo Scientific (Pittsburgh, USA).

Preparation of LMP Ink and OA LMP Ink: For the preparation of LMP ink, S80 and VitE were co-dissolved in methanol (MeOH) into a glass vial. Organic solvent was removed under reduced pressure (0.22 mbar for 24 h). The dried lipids were then mixed with weighed amounts of water. The mixture was centrifuged for 10 min at 5 000 g and manually mixed with a spatula. The procedure was repeated six times and the LMP was left to equilibrate for 48 h in the dark at room temperature. The uniformity of the ink was checked by visual inspection, ensuring that all the water phase was embedded into the gel matrix. For lipid mesophase containing the drug (OA-LMP ink), OA was added at a concentration of 2.5% w/w and dissolved with the lipid mixture. The subsequent steps followed the same procedure as outlined above.

Small Angle X-ray Scattering (SAXS): SAXS experiments were conducted to determine the phase identity and symmetry of LMP ink and the ensuing printlets with different percentages of S80, VitE and water, either empty or OA-loaded. The phase identity of the printlet was also evaluated after its incubation in HCl (pH 1.2) for 2 h. The measurements were carried out using a Bruker AXS Micro with a micro-focused X-ray source. The voltage and filament current were set to 50 kV and 1000 µA, respectively. The 2D Kratky collimator was used to collimate the Cu Kα radiation (λCu Kα = 1.5418 Å), and the data were collected by a 2D Pilatus 100K detector. The scattering vector Q, which was determined by the scattering angle 2θ and the wavelength λ, was calibrated using silver behenate. The data were collected and azimuthally averaged using the Saxsgui software to generate a 1D intensity versus scattering vector Q plot, with a Q range of 0.005 to 0.5 $Å^{-1}$. The samples were placed inside a stainless-steel cell between two thin replaceable mica sheets and sealed with an O-ring. The measurements were performed at 25 °C, and the samples were equilibrated for 10 min before measurements were taken. The scattered intensity was collected over a period of 30 min. Moreover, in case of the measurement carried out on the dissolution media (containing the dispersed printlet), these were performed at 37 °C. The samples were placed inside a 1.5 mm quartz capillary (Capillary Tube Supplies Ltd., United Kingdom) and equilibrated for 10 min and the scattered intensity was collected over a period of 2 h.

Design and 3D Printing: The design of the printlets was created using the Netfabb software (Autodesk, USA). A Bio-X bioprinter (Cellink, Sweden) with a pneumatic thermoplastic printhead was used for 3D printing the tablets. To ensure optimal results, ≈3 g of each formulation was placed into the pneumatic syringe and then centrifuged at 4′430 g for 15 min to remove any air bubbles. The following printing parameters were used: a pressure of 65 kPa; a print speed of 5 $mm^{-1}s$; and a nozzle diameter of 27G. The temperature was set to 25 °C, and the infill density was chosen as 13%, 25%, and 35% with a honeycomb pattern. After 3D printing, the manufactured printlets were allowed to dry at room temperature for 24 h, after which they were weighed, and their dimensions were measured

using a manual caliper. Moreover, to detect traces of methanol, the printlets were analyzed by headspace GC/HRMSGC (see Supporting Information).

Drug Load and Drug Distribution: To assess the homogeneity of drug distribution within the tablet matrix, a random selection of three OA-Printlets at all infill densities was taken, and each tablet was divided into three sections. Therefore, all sections were dissolved in MeOH, and drug concentration were analyzed and normalized based on a 10 mg weight. In contrast, to assess the equivalence of the total drug content between OA-Printlets with an infill density of 35% and the theoretical value–which corresponds to the marketed tablets (5 mg)–tablets were individually dissolved in 10 mL MeOH, and the drug concentration was quantified using high-performance liquid chromatography (HPLC; Ultimate 3000, Thermo Fisher Scientific, Switzerland) as already described.[61] Briefly, a Nucleosil 100–5 C_{18} column (250 × 4.0 mm, particle size 5 µm) (Macherey-Nagel, Düren, Germany) was used, and the mobile phase composition was 80% acetonitrile and 20% ultrapure water + 0.05% v/v o-phosphoric acid. The conditions for analysis were injection volume 20 µL, temperature 55 °C, flow rate 0.5 mL min^{-1} and detection wavelength 200 nm.

Rheological Characterization: The rheological characteristics of the printable lipid mesophase (LMP ink), as well as the printlets and OA-Printlets of various infill densities (13%, 25%, and 35%), were investigated using a Modular Compact Rheometer MCR 72 (Anton Paar, Graz, Austria) equipped with a cone-plate geometry, diameter = 49.942 mm and cone angle = 0.993°. The temperature was kept at 25 °C and the linear viscoelastic region (LVR) was determined by conducting an amplitude sweep at 1 Hz between 0.01 and 100% strain. The G′ (storage modulus) values reported in Figure 2d, were obtained by averaging the G′ value gained in a range of shear stress from 2 to 100 Pa (within the LVR). The flow point (τ_f) was indeed the value of the shear stress at the crossover point (G′ = G″). After, a frequency sweep was performed at a constant strain within the linear viscoelastic region between 0.1 and 100 rad s^{-1} at 25 °C.

Assessment of Self-Emulsification and Particle Size Determination: The self-emulsification properties of printlets were evaluated using an experimental setup consisting of a 50 mL tube and a custom-made metallic basket.[62] The evaluation was conducted in three different media: phosphate buffer saline (PBS) at pH 7.4, FaSSIF and FeSSIF to determine the disintegration of the tablets in intestinal fluids. To this end, printlets at various infill densities (13%, 25%, and 35%) were placed in 20 mL of the selected dissolution media and gently agitated using a shaker at 200 rpm, at a temperature of 37 °C for 2 h. The process of self-emulsification was visually assessed to examine the appearance of the resulting emulsions. After the self-emulsification assessment, aliquots of the bulk media were collected and analyzed using DLS. The mean hydrodynamic diameter of the dispersed species was determined using Litesizer 500 (Anton Paar, Graz, Austria) at a temperature of 25 °C and a backscatter angle of 175° and a 658 nm laser. The number of measurements was 6 while a refractive index of 1.3304 and a viscosity of 0.89 mPa s^{-1} were set for the solvent. The samples were analyzed without additional dilution and since their high polydispersity, the autocorrelation functions (which do not show a mono exponential decay) were fitted by CONTIN algorithmic.

Transmission Electron Cryomicroscopy (Cryo-TEM): To obtain images of the colloidal structures formed during the dissolution into simulated digestive fluids, a printlet was subjected to the aforementioned three different media, namely PBS, FaSSIF, and FeSSIF, for a duration of 2 h. The resulting media was subsequently diluted to a concentration of 1 mg mL^{-1} of S80 and analyzed using cryo-TEM. To obtain images of printlets in simulated digestive fluids enriched with pancreatin, printlets were first kept in HCl for 1 h (at pH 1.2) in a metal mesh basket and then transferred into a biorelevant media (FaSSIF) enriched with pancreatin. Samples were taken at 2, 4, and 6 h and immediately after sampling plunge frozen, without dilution. Lacey carbon films mounted on Cu 200 mesh grids (Agar Scientific, UK) served as the substrate for sample deposition. Initially, these grids were subjected to plasma cleaning at 220 V and 0.15 mBar vacuum for a duration of 7 s. Subsequently, a 4 µL aliquot of the sample was pipetted onto the front side of the prepared grids. For the samples, the blotting chamber was pre-conditioned to a controlled environment of 21 °C and 100% humidity. PBS and FaSSIF samples were plunge-frozen using a Vitrobot (FEI, USA). In contrast, the FeSSIF sample was prepared using an EM GP2 Automatic Plunge Freezer (Leica, Germany). Excess liquid from these samples was automatically blotted away using two strips of filter paper and blot time of 2 × 4 s was employed (1 × 4 s was employed for samples originating from fluids enriched with pancreatin), followed by immediate plunge-freezing into liquid ethane maintained at −180 °C. The prepared grids were then stored in liquid nitrogen until they were ready for Transmission Electron Microscopy (TEM) observation. Low-dose electron diffraction studies were carried out using an FEI Tecnai Spirit F20 electron microscope (FEI, USA). Imaging was performed at an acceleration voltage of 80 kV, and the captured images were recorded using an FEI Eagle CCD Camera (FEI, USA).

Equilibrium Solubility Measurements: The following method was adapted from a previous study.[63] OA solubility was carried out in the following media: PBS, FaSSIF, and FeSSIF. The impact of the formulation on the drug solubility was assessed by using the experimental setup both with and without the formulation. Free OA (10 mg) or the correspondent amount of formulation (OA-Printlet) containing 10 mg of drug was added to 5 mL of the dissolution medium in glass vials. The vials were incubated at 37 °C for 24 h at 200 rpm, after which 1 mL was transferred in an Eppendorf tube and centrifuged for 10 min at 6′800 g. The supernatant was lyophilized and diluted to an appropriate concentration for HPLC analysis to determine the drug concentration.

In Vitro Drug Release Experiment: The release profile of OA from the printlet with an infill density of 35% was performed in the custom-made metallic basket.[62] The baskets with the printlets (n = 3) were placed in tubes containing 20 mL of PBS (pH 7.4) and this setup was placed in a shaking incubator at 37 °C and 200 rpm. At determined time intervals (0.5, 1, 2, 3, 4, 5, and 6 h), the release medium was collected and replaced with 20 mL fresh PBS. Aliquots of 5 mL were lyophilized and resuspended in mobile phase, and the drug content was determined by HPLC-UV as already described above.[61] The same apparatus was applied to assess the disintegration behaviour of the printlet and the drug release in biorelevant media. The baskets with the printlets were first placed in tubes containing 25 mL of HCl (0.1 M) for 1 h and then in tubes containing 25 mL of FaSSIF enriched with pancreatin for 1 h, 3 h and 6 h (n = 3), as described in literature.[57] The setup was placed in a shaking incubator at 37 °C and 200 rpm. After the time intervals, the residual formulation in the basket was dissolved in methanol, and the drug content was determined by HPLC-UV as described above.[61]

Cell Culture Conditions and Cell Assays: Caco-2 cells were grown in a culture medium of DMEM with 4.5 g/L glucose, L-glutamine & sodium pyruvate, and it was supplemented with 10% FBS, 1% NEAA, and 1% P/S (Penicillin/Streptomycin). The cells were maintained in T-75 flasks in the growth medium and used at passage 11 for the experiments, after being recovered from cryogenic storage. To assess the cytotoxicity of the formulation, Caco-2 cells were seeded in 96-well plates at a density of 2 x 10^4 cells per well in a final volume of 200 µL of culture medium. The cells were cultured for 18 days, with the medium changed every two days.

LX-2 cells (Merck Millipore, USA) were cultured in high glucose (4.5 g L^{-1}) DMEM (Carl Roth, Germany) supplemented with 10 000 units L^{-1} of penicillin and streptomycin (P/S; Gibco, USA), 200 mM L-Glutamine (Sigma, USA), and 2% (v/v) of sterile filtered (0.2 µm, cellulose acetate membrane) FBS (Merck Millipore, USA) at 37 °C in a humidified atmosphere containing 5% CO_2. Cells at passage 10 were used for experiments and treated with either single components of the formulation or the final formulation, which was diluted with culture medium to reach final concentrations of 0.076% w/v of printlet or OA-Printlet, 0.052% of S80, 0.002% w/v of OA, 0.01% of VitE in a 24-well plate to analyze mRNA transcription (vide infra), in a 48-well plate for the lipid droplet content analysis using Oil Red O staining and in a 96-well plate for the CCK-8 assay (Merck Millipore, USA). For the mRNA transcription, 60′000 cells/well were seeded in 0.5 mL full growth medium (High glucose DMEM + 2% (v/v) FBS + 2 mM L-glutamine + 1% (v/v) P/S), for the lipid droplet content analysis 30 000 cells $well^{-1}$ were seeded in 0.2 mL full growth medium (High glucose DMEM + 2% (v/v) FBS + 2 mM L-glutamine + 1% (v/v) P/S). For the CCK-8 assay 10′000 cells/well were seeded in 0.1 mL full growth medium (High glucose DMEM + 2% (v/v) FBS + 2 mM

L-glutamine + 1% (v/v) P/S) and incubated in a culture incubator at 37 °C constant with a humidified atmosphere of 5% of CO_2.

MTT Colorimetric Assay: Caco-2 cells were then treated with either single components of the formulation or the final formulation, which was diluted with culture medium to a final volume of 200 µL per well in 96-well plates. The following final concentrations were achieved: 0.076% w/v of printlet or OA-Printlet, 0.052% of S80, 0.002% w/v of OA, 0.01% of VitE for 24 h. After treatments, the viability of the Caco-2 cells was evaluated using the MTT colorimetric assay. For MTT assay, cells were incubated with 5 mg mL^{-1} of MTT solution for 3 h in a cell culture incubator at 37 °C constant with a humidified atmosphere of 5% of CO_2. Upon completion of incubation, the medium was replaced with DMSO (200 µL $well^{-1}$) to solubilize the formazan crystals product. This last quantity was analyzed through the optical density (OD) using a microplate reader NB-12-0035, NeoBiotech (Nanterre, France) at a wavelength of 540 nm.

Monolayer Integrity Assessment: To assess the effect of a self-emulsified formulation on the integrity of Caco-2 cell monolayer, a Lucifer Yellow (LY) assay was employed. Caco-2 cells were cultured in 12-well plates on Transwell cellQART inserts for 21 days at a seeding density of 2.5×10^5 cells per well, with 500 µL of DMEM added to the apical side and 1.5 mL of DMEM to the basolateral side. On the day of treatment, cells were exposed to either a single component of the formulation or the final formulation, diluted in culture medium to a final volume of 500 µL per well and added to the apical side of the Transwell cellQART. The final concentrations employed corresponded to those established for the cell viability assay. Samples (200 µL) were collected from the basolateral side of the Transwell cellQART at 30-min intervals for a total of 4 h. The fluorescence of the samples was measured at excitation 485 nm and emission 535 nm using the Infinite 200 PRO Tecan (Männedorf, Switzerland) plate reader to assess the paracellular transport of the fluorescent dye LY and hence the integrity of the Caco-2 cell monolayer.

Cell Counting Kit-8 Assay: LX-2 (10 000 cells) were seeded in a 96-well plate (Faust, Switzerland). The CCK-8 assay (Merck Millipore, USA) was used to determine cell viability and was used following manufacturer's guidelines. Briefly, post-treatment, cells were washed with PBS. Then, 90 µL FBS-free medium and 10 µL CCK-8 solution were added into the well. After 2 h of incubation at 37 °C and 5% CO_2, absorbance at 450 nm was measured using an Infinite M Pro 200F-PlexNano microplate reader (Tecan, Switzerland). The viability was normalized to LX-2 cells treated with the vehicle (FBS-free DMEM).

ORO Staining: LX-2 (30 000 cells) were seeded in a 48-well plate (Faust, Switzerland) for lipid droplet analysis, adapted from previous method.[29] Cells were washed, fixed (200 µL $well^{-1}$ Roti-Histofix 4% for 10 min at RT), and washed with 1 mL $well^{-1}$ deionized MilliQ water. Staining: 200 µL $well^{-1}$ filtered (0.45 µm) Oil Red O (ORO, 0.5% w/v) in propylene glycol for 15 min at RT. After ORO removal, cells were washed twice with PBS. The nuclei were stained with 200 µL $well^{-1}$ 4 µM DAPI solution in PBS for 5 min at RT. Cells were rinsed with PBS and imaged using a Nikon Ti-U microscope (bright field, DAPI and Texas Red filters). FIJI software was used for fluorescent binary area and cell count analysis, determining lipid droplets [μm^2]/cell.

qPCR: LX-2 (60 000 cells) were seeded in a 24-well plate (Faust, Switzerland). Post-treatment, TRIzol reagent (Thermofischer, USA) was used to isolate total RNA per instructions.[64] Briefly, cells lysed with TRIzol in the plate were transferred to Axygen tubes (Corning, USA). Chloroform (1/5 TRIzol volume) was added, followed by vortexing and 20 min centrifugation (4 °C, 16 000 g; Hermle Z 366 K centrifuge, Faust, Switzerland). The upper phase was moved to a new tube, and glycogen (Merck Millipore, USA) and isopropanol (Biosolve, Netherlands) were added. RNA precipitated on ice, was pelleted (10 min, 4 °C, 24 000 g), washed with 70% EtOH, and resuspended in DEPC-treated MilliQ-water. RNA concentration was measured using a NanoDrop (Thermo Fisher, USA). RNA reverse transcription to cDNA: 1000 ng RNA was mixed with random hexamer (Microsynth, Switzerland), incubated (65 °C, 5 min), mixed with a master mix (5 µL reverse transcriptase buffer 10x (Agilent, USA), 5 µL 100 mM DTT (Stratagene, USA), 2 µL 10 mM dNTPs (Thermo Fisher, USA), 0.5 µL 40 U μL^{-1} RiboLock RNase inhibitor (Fermentas, Germany), 1 µL reverse transcriptase 200 rxn (Agilent, USA), incubated at RT for 10 min, followed by incubations for 1 h at 50 °C and 20 min at 75 °C. Afterwards water was added to achieve 8 ng/µL cDNA. Primers (see Supporting Information, Table S6, Supporting Information) were diluted in MilliQ to 2.5 µM primer pair solution. qPCR was performed with Brilliant III Ultra-fast SYBR Green qPCR master mix (MM; Agilent, USA). A pipetting robot (Qiagen, Germany) was used to pipette the samples (3 µL cDNA, 7.5 µL 2x MM, 3 µL primer mix, 1.5 µL water). Samples were transferred to a qPCR analyzer centrifuge (Qiagen, Germany) for 40 cycles (95 °C and 60 °C, fluorescence measured at 60 °C). A melting curve was obtained after the 40 cycles. Rotor Gene Q software and Excel was used to analyze the data. The qPCR data was analyzed using the delta delta CT method for quantitative real-time polymerase chain reaction using GAPDH as normalizer gene.

Statistical Analysis: The obtained data are presented as mean ± standard deviation (STDV). All performed expertiments were replicated at least three times ($n = 3$). $*p < 0.05$, $**p < 0.01$, $***p < 0.001$ as determined by one-way ANOVA with multiple comparisons and Tukey correction. All tests were performed using Prism (GraphPad) and applying default settings for the above-mentioned analyses.

Supporting Information

Supporting Information is available from the Wiley Online Library or from the author.

Acknowledgements

R.G. and M.C. contributed equally to this work. The authors would like to thank Dr. Nasif, Nicole Kleinschmidt, and Prof. Dr. Mühlemann from the University of Bern for their support on the qPCR experiments. Cryogenic electron microscopy sample preparation and imaging were performed with devices supported by the Microscopy Imaging Centre (MIC) of the University of Bern. Prof. Dr. Stefan Schürch and Claudia Bühr are kindly acknowledged for the MS analysis. Dr. Serena Rosa Alfarano (Laboratory of Food & Soft Materials, Institute of Food, Nutrition and Health, IFNH; Department for Health Sciences and Technology, D-HEST, ETH Zurich Switzerland) is kindly acknowledged for the precious support during the SAXS experiments.

Open access funding provided by Universitat Bern.

Conflict of Interest

The authors declare no conflict of interest.

Data Availability Statement

The data that support the findings of this study are available from the corresponding author upon reasonable request.

Keywords

3D-printing, gastro-resistant oral dosage form, lipid-based formulations, lipidic mesophases, self-emulsification

Received: December 11, 2023
Published online:

[1] C. J. H. Porter, N. L. Trevaskis, W. N. Charman, *Nat. Rev. Drug Discovery* **2007**, *6*, 231.

[2] O. M. Feeney, M. F. Crum, C. L. McEvoy, N. L. Trevaskis, H. D. Williams, C. W. Pouton, W. N. Charman, C. A. S. Bergström, C. J. H. Porter, *Adv. Drug Delivery Rev.* **2016**, *101*, 167.
[3] R. G. Strickley, *Oral Lipid-Based Formula* (Ed.: D. J. Hauss), CRC Press, Boca Raton **2007**, p. 54.
[4] T. O. Tang, S. Holmes, B. J. Boyd, G. P. Simon, *Biomater. Adv.* **2022**, *137*, 212818.
[5] T. Tracy, L. Wu, X. Liu, S. Cheng, X. Li, *Int. J. Pharm.* **2023**, *631*, 122480.
[6] H. G. Yi, Y. J. Choi, K. S. Kang, J. M. Hong, R. G. Pati, M. N. Park, I. K. Shim, C. M. Lee, S. C. Kim, D. W. Cho, *J. Controlled Release* **2016**, *238*, 231.
[7] I. Seoane-Viaño, J. J. Ong, A. Luzardo-Álvarez, M. González-Barcia, A. W. Basit, F. J. Otero-Espinar, A. Goyanes, *Asian J. Pharm. Sci.* **2021**, *16*, 110.
[8] K. Vithani, A. Goyanes, V. Jannin, A. W. Basit, S. Gaisford, B. J. Boyd, *Pharm. Res.* **2019**, *36*, 102.
[9] N. Sandler, M. Preis, *Trends Pharmacol. Sci.* **2016**, *37*, 1070.
[10] S. A. Khaled, J. C. Burley, M. R. Alexander, J. Yang, C. J. Roberts, *J. Controlled Release* **2015**, *217*, 308.
[11] H. Windolf, R. Chamberlain, J. Breitkreutz, J. Quodbach, *Pharmaceutics* **2022**, *14*, 931.
[12] B. W. Barber, C. Dumont, P. Caisse, G. P. Simon, B. J. Boyd, *Pharmaceutics* **2021**, *13*, 2107.
[13] B. Zhang, X. Y. Teoh, J. Yan, A. Gleadall, P. Belton, R. Bibb, S. Qi, *Int. J. Pharm.* **2022**, 625.
[14] W. J. Goh, S. X. Tan, G. Pastorin, P. C. L. Ho, J. Hu, S. H. Lim, *Int. J. Pharm.* **2021**, *598*, 120360.
[15] H. M. Jeong, K. Y. Weon, B. S. Shin, S. Shin, *Molecules* **2020**, *25*, 454.
[16] T. Charoenying, P. Patrojanasophon, T. Ngawhirunpat, T. Rojanarata, P. Akkaramongkolporn, P. Opanasopit, *J. Drug Deliv. Sci. Technol.* **2020**, *55*, 101393.
[17] A. Melocchi, M. Uboldi, F. Briatico-Vangosa, S. Moutaharrik, M. Cerea, A. Foppoli, A. Maroni, L. Palugan, L. Zema, A. Gazzaniga, *Pharmaceutics* **2021**, *13*, 759.
[18] A. P. Haring, Y. Tong, J. Halper, B. N. Johnson, *Adv. Healthcare Mater.* **2018**, *7*, 12.
[19] Y. Yang, X. Wang, X. Lin, L. Xie, R. Ivone, J. Shen, G. Yang, *Int. J. Pharm.* **2020**, *583*, 119360.
[20] Aprecia Pharmaceuticals Company, https://spritam.com
[21] L. Krueger, J. A. Miles, A. Popat, *J. Controlled Release* **2022**, *351*, 444.
[22] J. Firth, A. W. Basit, S. Gaisford, in *AAPS Advances in the Pharmaceutical Sciences Series* (Eds.: A. W. Basit, S. Gaisford), Springer, Berlin, Heidelberg **2018**, pp. 133–151.
[23] I. Seoane-Viaño, P. Januskaite, C. Alvarez-Lorenzo, A. W. Basit, A. Goyanes, *J. Controlled Release* **2021**, *332*, 367.
[24] S. Aleandri, R. Mezzenga, *Phys. Today* **2020**, *73*, 38.
[25] W. K. Fong, T. Hanley, B. J. Boyd, *J. Controlled Release* **2009**, *135*, 218.
[26] K. W. Y. Lee, T. H. Nguyen, T. Hanley, B. J. Boyd, *Int. J. Pharm.* **2009**, *365*, 190.
[27] R. Negrini, R. Mezzenga, *Langmuir* **2011**, *27*, 5296.
[28] M. Carone, M. R. Spalinger, R. A. Gaultney, R. Mezzenga, K. Hlavačková, A. Mookhoek, P. Krebs, G. Rogler, P. Luciani, S. Aleandri, *Nat. Commun.* **2023**, *14*, 3489.
[29] G. Valentino, C. Zivko, F. Weber, L. Brülisauer, P. Luciani, *Pharmaceutics* **2019**, *11*, 676.
[30] Y. D. A. Dong, I. Larson, T. Hanley, B. J. Boyd, *Langmuir* **2006**, *22*, 9512.
[31] L. Bitan-Cherbakovsky, I. Yuli-Amar, A. Aserin, N. Garti, *Langmuir* **2009**, *25*, 13106.
[32] L. Sagalowicz, S. Guillot, S. Acquistapace, B. Schmitt, M. Maurer, A. Yaghmur, L. De Campo, M. Rouvet, M. Leser, O. Glatter, *Langmuir* **2013**, *29*, 8222.
[33] R. Mezzenga, C. Meyer, C. Servais, A. I. Romoscanu, L. Sagalowicz, R. C. Hayward, *Langmuir* **2005**, *21*, 3322.
[34] G. Montalvo, M. Valiente, E. Rodenas, *Langmuir* **1996**, *12*, 5202.
[35] N. M. Bandarra, R. M. Campos, I. Batista, M. L. Nunes, J. M. Empis, *JAOCS, J. Am. Oil Chem. Soc.* **1999**, *76*, 905.
[36] S. M. Smith, A. H. Pegram, *J. Pharm. Technol.* **2017**, *33*, 66.
[37] https://www.ema.europa.eu/en/medicines/human/EPAR/ocaliva#authorisation-details-section.
[38] B. A. Neuschwander-Tetri, R. Loomba, A. J. Sanyal, J. E. Lavine, M. L. Van Natta, M. F. Abdelmalek, N. Chalasani, S. Dasarathy, A. M. Diehl, B. Hameed, K. V. Kowdley, A. McCullough, N. Terrault, J. M. Clark, J. Tonascia, E. M. Brunt, D. E. Kleiner, E. Doo, *Lancet* **2015**, *385*, 956.
[39] S. Cipriani, A. Mencarelli, G. Palladino, S. Fiorucci, *J. Lipid Res.* **2010**, *51*, 771.
[40] P. Fickert, A. Fuchsbichler, T. Moustafa, M. Wagner, G. Zollner, E. Halilbasic, U. Stöger, M. Arrese, M. Pizarro, N. Solís, G. Carrasco, A. Caligiuri, M. Sombetzki, E. Reisinger, O. Tsybrovskyy, K. Zatloukal, H. Denk, H. Jaeschke, M. Pinzani, M. Trauner, *Am. J. Pathol.* **2009**, *175*, 2392.
[41] L. Verbeke, R. Farre, J. Trebicka, M. Komuta, T. Roskams, S. Klein, I. Vander Elst, P. Windmolders, T. Vanuytsel, F. Nevens, W. Laleman, *Hepatology* **2014**, *59*, 2286.
[42] C. Zivko, F. Witt, A. Koeberle, G. Fuhrmann, P. Luciani, *Eur. J. Pharm. Biopharm.* **2023**, *182*, 32.
[43] P. P. Hoppe, G. Krennrich, *Eur. J. Nutr.* **2000**, *39*, 183.
[44] I. Martiel, N. Baumann, J. J. Vallooran, J. Bergfreund, L. Sagalowicz, R. Mezzenga, *J. Controlled Release* **2015**, *204*, 78.
[45] S. Committee, O. N. Toxicity, T. H. E. Environment, **1999**, *0051*, 17.
[46] M. Mendozza, L. Caselli, C. Montis, S. Orazzini, E. Carretti, P. Baglioni, D. Berti, *J. Colloid Interface Sci.* **2019**, *541*, 329.
[47] J. L. Jones, T. C. B. McLeish, *Langmuir* **1995**, *11*, 785.
[48] S. Radiman, C. Toprakcioglu, T. McLeish, *Langmuir* **1994**, *10*, 61.
[49] W. K. Fong, R. Negrini, J. J. Vallooran, R. Mezzenga, B. J. Boyd, *J. Colloid Interface Sci.* **2016**, *484*, 320.
[50] S. Salentinig, L. Sagalowicz, O. Glatter, *Langmuir* **2010**, *26*, 11670.
[51] D. Riethorst, P. Baatsen, C. Remijn, A. Mitra, J. Tack, J. Brouwers, P. Augustijns, *Mol. Pharmaceutics* **2016**, *13*, 3484.
[52] N. Lupo, C. Steinbring, J. D. Friedl, B. Le-Vinh, A. Bernkop-Schnürch, *Drug Dev. Ind. Pharm.* **2021**, *47*, 22.
[53] B. J. Boyd, S. M. Khoo, D. V. Whittaker, G. Davey, C. J. H. Porter, *Int. J. Pharm.* **2007**, *340*, 52.
[54] R. Lalge, N. Kaur, N. K. Duggirala, R. Suryanarayanan, *Mol. Pharmaceutics* **2022**, *19*, 2595.
[55] M. Atanacković, M. Poša, H. Heinle, L. Gojković-Bukarica, J. Cvejić, *Colloids Surf., B* **2009**, *72*, 148.
[56] Lancaster (12), *US 10, 751, 349 B2.*
[57] L. C. Alskär, J. Keemink, J. Johannesson, C. J. H. Porter, C. A. S. Bergström, *Mol. Pharmaceutics* **2018**, *15*, 4733.
[58] R. Konsoula, F. A. Barile, *Toxicol. Vitr.* **2005**, *19*, 675.
[59] C. Zivko, K. Fuhrmann, G. Fuhrmann, P. Luciani, *Commun. Biol.* **2022**, *5*, 1155.
[60] T. F. Lee, K. M. Mak, O. Rackovsky, Y. L. Lin, A. J. Kwong, J. C. Loke, S. L. Friedman, *J. Cell. Physiol.* **2010**, *223*, 648.
[61] M. Douša, M. Slavíková, T. Kubelka, J. Černý, P. Gibala, J. Zezula, *J. Pharm. Biomed. Anal.* **2018**, *149*, 214.
[62] L. S. Karfeld-Sulzer, C. Ghayor, B. Siegenthaler, M. De Wild, J. C. Leroux, F. E. Weber, *J. Controlled Release* **2015**, *203*, 181.
[63] A. Abdalla, S. Klein, K. Mäder, *Eur. J. Pharm. Sci.* **2008**, *35*, 457.
[64] A. A. Ganguin, I. Skorup, S. Streb, A. Othman, P. Luciani, *Adv. Healthcare Mater.* **2023**, *12*, 2300811.